Supplementary Figure 1. Sequence of region in *P. laumondii* TTO1 containing predicted *arcZ* sequence

Supplementary Figure 2. The ArcZ and Hfq regulon in *P. laumondii*

Supplementary Figure 3. RIPseq enrichment around the region of *hexA*

Supplementary Figure 4. 5' UTR of *hexA* including predicted ArcZ binding site

Supplementary Figure 5. Alignment of the *hexA* 5' UTR from different species

Supplementary Notes

Supplementary Note 1. Hfq is involved in SM biosynthesis in *Xenorhabdus.* To confirm if Hfq is also involved in SM regulation in *Xenorhabdus*, we created a knockout of *hfq* in *X. szentirmaii* DSM16338 and performed HPLCMS/MS and RNAseq on the confirmed deletion strains (Supplementary Table 1). In contrast to *Photorhabdus*, the *X. szentirmaii* Δ*hfq* strain only revealed 312 coding sequences significantly regulated compared to the wild type at mid-exponential phase. In accordance with our hypothesis, *hexA* was significantly upregulated (8.4x, FDR<0.01, Supplementary Table 1). Consistent with this observation, the production of nearly all known SMs were decreased (Figure 3e), suggesting a conserved mode of action in *Xenorhabdus*.

Supplementary Note 2. Identification of sRNAs in *Photorhabdus* and *Xenorhabdus.* Only very little is known about sRNAs from entomopathogenic bacteria. To identify potential Hfq-binding sRNAs and consequently the Hfq-based regulation of SMs in general, we sequenced the RNA of *P. laumondii* (formerly *P. luminescens*) and *X. szentirmaii* using a library preparation protocol specific for sRNAs. Sequences of the sRNAs from two libraries from each of *Photorhabdus* and *Xenorhabdus* yielded a total of 26,784,563 (13,204,857 and 13,579,706) and 28,813,442 (13,472,683 and 15,340,759) raw reads, respectively. Additionally, we prepared samples from *X. szentirmaii* for CappableSeq, a protocol that differentiates between primary and secondary transcripts [1]. We recently reported a data set from *P. laumondii*, which identified 15,500 primary and 3,741 secondary transcripts [2]. Here, we reanalyzed these data using stricter cutoff criteria (see Methods) resulting in a total of 6,174 TSSs. The *X. szentirmaii* CappableSeq data led to the identification of 2,196 TSSs (Supplementary Table 2).

By combining data from the CappableSeq experiments data along with RNAseq data from Δ*hfq* and wild type strains (also Δ*hfq*Δ*hexA* and Δ*hfq*::*hfq* in *Photorhabdus* from our previous study[3]), we were able to annotate putative transcripts, 5'-untranslated regions (UTRs), 3'-UTRs and sRNAs using ANNOgesic[4] (Supplementary Table 17 and 18). The annotated sRNAs were added to those described in the Bacterial sRNA Database (BSRD)[5] yielding a total of 280 and 130 candidates for sRNAs in *Photorhabdus* and *Xenorhabdus*, respectively (Supplementary Table 17 & 18).

Supplementary Note 3. Transposon mutant library screen. A transposon mutant library was constructed to identify genes defective in SM production. Many of the analysed mutant strains showed severely reduced SM production titers in comparison to the WT strain. In most cases, multiple SM classes were affected by the transposon insertion (Extended Data Figure 3). On rare occasions, the transposon insertion led to an increase in production of certain SMs. For example, dmPLA-A and MVAP levels were elevated in mutant strain 9 and IPS titers were slightly raised in the TN-mutant strains 10 and 11. Interestingly, the remaining SMs were negatively affected in those strains. As the growth appeared to be affected by the transposon insertion (Supplementary Table 6, it remains uncertain how the growth defects correlate with SM production. For further analysis, we decided to focus on strain 3 that showed only moderate growth defects while at the same time producing reduced SM titers, consistent with the phenotype of the *hfq* deletion mutant.

Supplementary Note 4. The ArcZ regulon in *Photorhabdus* and *Xenorhabdus.* Since there is a clear overlap between the regulons and functions of Hfq and ArcZ, we performed RNAseq on the Δ*arcZ* strains of *P. laumondii* and *X. szentirmaii*, as well as on their respective knock-in

complementation mutants. RNAseq analysis on the deletion of *arcZ* in *Photorhabdus* revealed an even broader effect than in our Δ*hfq* mutant, significantly affecting the transcriptional level of 735 coding sequences in *P. laumondii* (FDR<0.01; $\log_2$ fold change >2, Figure 4a, Supplementary Table 7 & 8). In *X. szentirmaii*, a global effect of the *arcZ* deletion was also observed, albeit only 191 genes were affected in this strain (Supplementary Table 12). In both deletion strains however, the majority of affected coding sequences were downregulated (Figure 4a & b, Supplementary Table 8 & 12). In an attempt to identify broader effects, we grouped all the genes that were significantly changed into eight different categories based on their known or proposed function: SM, regulators, virulence, phage related, cell wall, cell processes, hypothetical proteins and unknown. We first included only those genes that were significantly regulated in the *arcZ* deletion mutant and not in the *hfq* deletion mutant (Supplementary Figure 2a). In all cases (except for virulence related and unknown) a clear trend towards downregulation of the transcriptional level could be observed in the deletion of *arcZ*. This trend was also observed in the *hfq* deletion mutant, although somewhat weakened compared to the *arcZ* deletion strain. The knock-in complementation restored the vast majority of observed changes back to WT level (Supplementary Figure 2a). Finally, we looked at genes whose expression was significantly altered in both the *arcZ* and *hfq* deletion strain. The individual categories clustered very closely together as indicated by the median (Supplementary Figure 2b).

Supplementary Note 5. Effect of *arcZ* deletion in *Xenorhabdus.* The drastic reduction in SMs in the deletion mutant was restored with a knock-in complementation of *arcZ* (Figure 3e). We also observed that protoporphyrin IX (PPIX), the direct precursor for heme, was highly overproduced (~30-fold) in the Δ*arcZ* strain of *X. szentirmaii* compared to the WT, suggesting

that the regulatory functions of ArcZ in *Photorhabdus* and *Xenorhabdus* possibly go beyond SM production. Since heme is reported to play an important role in nematode growth and development, we used the deletion mutants and complemented strains and performed nematode development assays. Both the WT and Δ*arcZ* strain of *X. szentirmaii* were able to support nematode development after 4 days of inoculation. However, the Δ*arcZ* strain of *P. laumondii* showed a significantly reduced capability to support nematode development (Extended Data Figure 4), consistent with our data showing that isopropylstilbene falls under the Hfq-ArcZ regulatory umbrella (Figure 4a, Supplementary Tables 7 & 8).

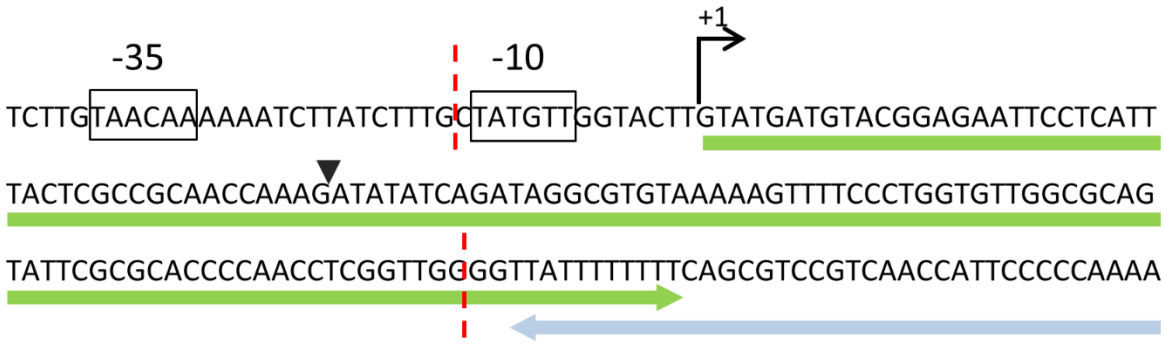

Supplementary Figure 1. Sequence of region in *P. laumondii* TTO1 containing predicted *arcZ* sequence (green arrow). The 3' end of *arcB* (blue arrow) is also shown. Dotted red lines indicate region of *arcZ* that was deleted. Also indicated is the site of insertion from transposon sequencing (inverted black triangle), as well as the -35 and -10 promotor regions and the transcriptional start site (+1).

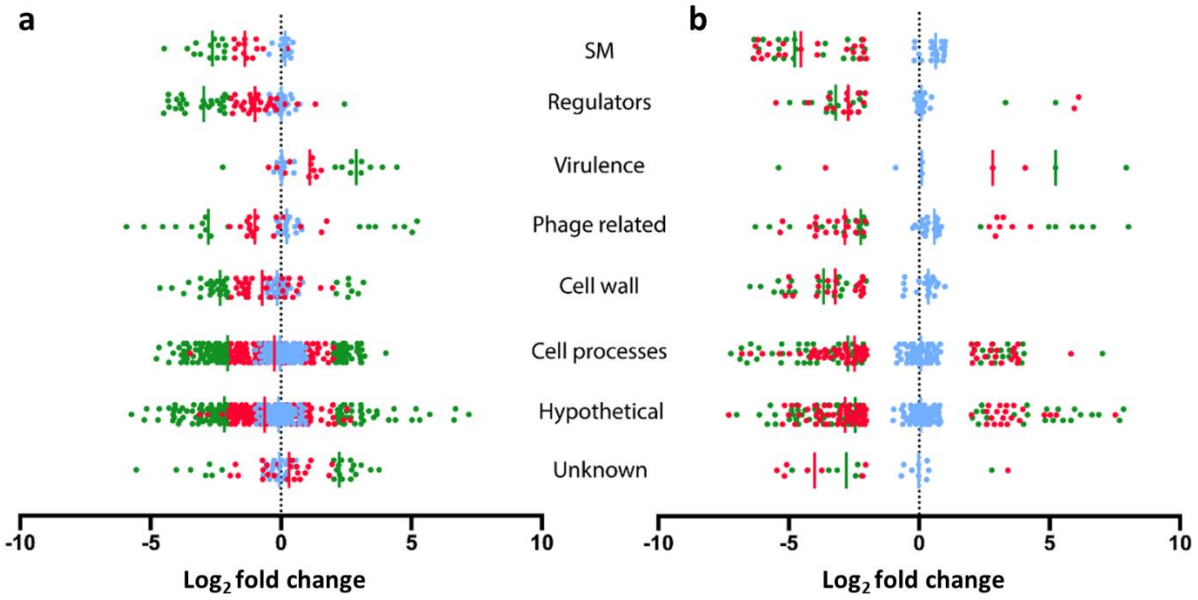

Supplementary Figure 2a. Genes that were significantly affected in the Δ*arcZ* strain and not the Δ*hfq* strain or **b** affected in both Δ*arcZ* and Δ*hfq* strains. The coding sequences associated with Δ*arcZ* of *P. laumondii* (green), Δ*hfq* (red) or Δ*arcZ::arcZ* (blue) compared to the WT were grouped into eight different categories: specialized metabolites (SM), regulators, virulence, phage related, cell wall, cell processes, hypothetical and unknown based on their annotations. Vertical lines represent the median for each group. Complete lists of regulated genes for *P. laumondii* mutants can be seen in Supplementary Tables 14-15.

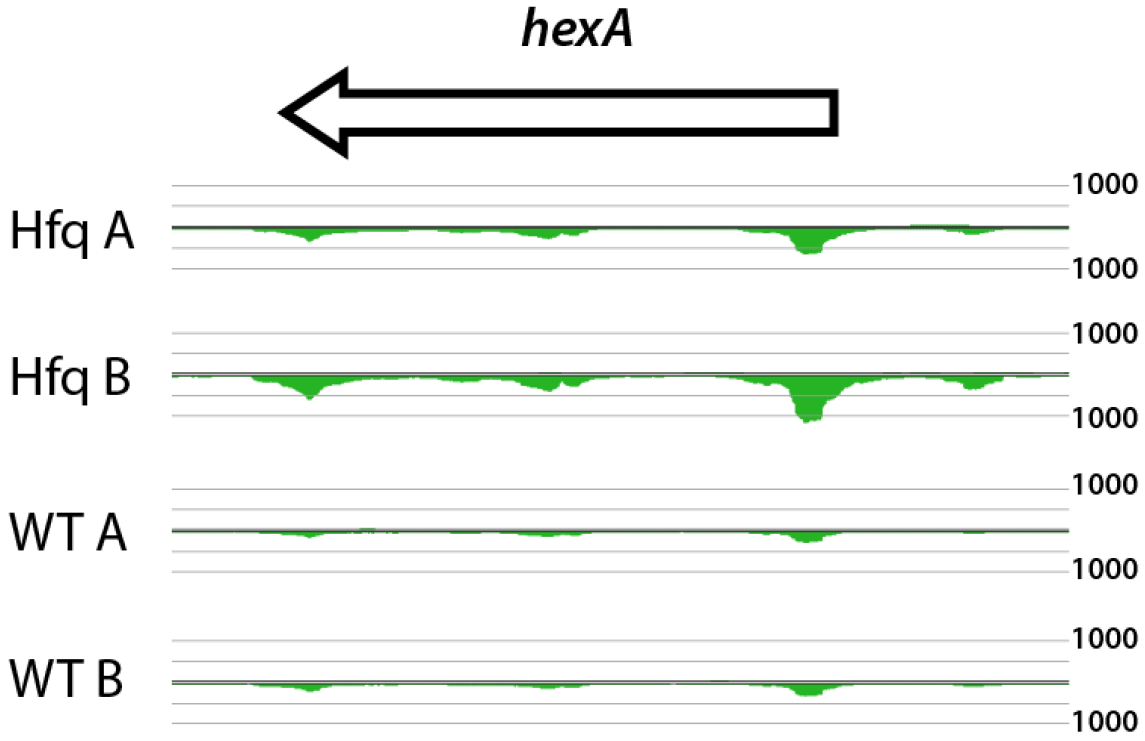

Supplementary Figure 3. RIPseq enrichment around the region of *hexA* in Hfq^{3xFLAG} samples (Hfq A & B) and untagged samples (WT A & B). Plots indicate the strand reads map to (bottom = reverse, top = forward). Scale represents perfectly mapped reads. For all enriched regions, see Supplementary Tables 11 and 12.

a HexA_UTR

ATGTTAATTTAATTTGATAGTGCTTACGTAAA**AACACCAGG**TTAGTTAGTAATTA

AAATCAAAAAAAAGTGATGAATAAACAATG

b HexA_PacI_UTR

ATGTTAATTTAATTTGATAGTGCTTACGTAAA**TTAATTAA**TTAGTTAGTAATTAAA

ATCAAAAAAAAGTGATGAATAAACAATG

Supplementary Figure 4a 5'-UTR of *hexA* including the predicted ArcZ binding site (red). The arrow indicates the start of the *hexA* coding sequence. **b** The predicted ArcZ binding site (AACACCAGG) was exchanged to a *Pac*I restriction site (TTAATTAA) as shown.

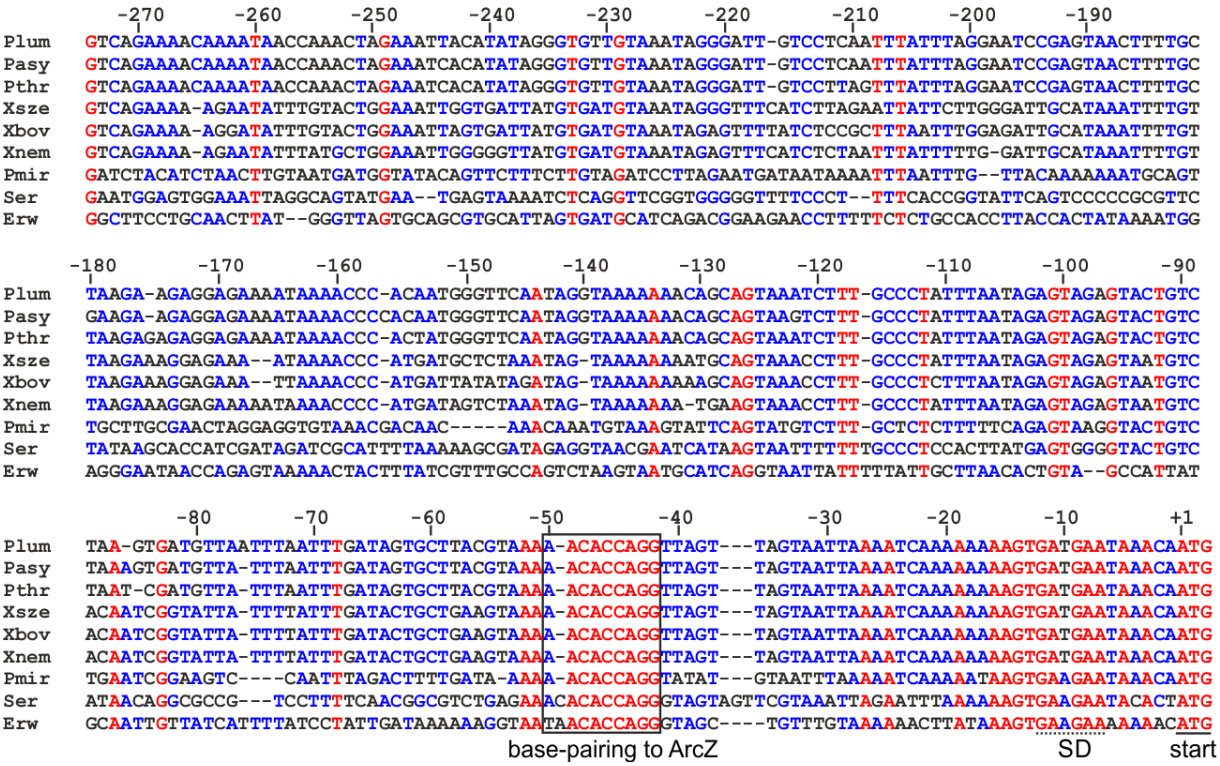

Supplementary Figure 5. Alignment of the *hexA* 5' UTR from *P. laumondii* TT01, *P. asymbiotica*, *P. thracensis*, *X. szentirmaii*, *X. bovienii*, *X. nematophila*, *Proteus mirabilis*, *Serratia marcescens* and *Erwinia* sp. J780, beginning with the transcriptional start site. The sequences were aligned using the Multalin Algorithm[21]. Black box indicates the region of base-pairing to ArcZ. SD sequence and start codon of *hexA* are underlined. Numbers indicate distance to the start codon.

References

1. Ettwiller, L., Buswell, J., Yigit, E. & Schildkraut, I. A novel enrichment strategy reveals unprecedented number of novel transcription start sites at single base resolution in a model prokaryote and the gut microbiome. *BMC Genomics* **17,** 199 (2016).
2. Tobias, N. J., Linck, A. & Bode, H. B. Natural Product Diversification Mediated by Alternative Transcriptional Starting. *Angew. Chem. Int. Ed. Engl.* **57,** 5699–5702 (2018).
3. Tobias, N. J. *et al. Photorhabdus*-nematode symbiosis is dependent on *hfq*-mediated regulation of secondary metabolites. *Environ. Microbiol.* **19,** 119–129 (2017).
4. Yu, S.-H., Vogel, J. & Förstner, K. U. ANNOgesic: a Swiss army knife for the RNA-seq based annotation of bacterial/archaeal genomes. *Gigascience* **7,** 673 (2018).
5. Li, L. *et al.* BSRD: a repository for bacterial small regulatory RNA. *Nucleic Acids Res.* **41,** D233–D238 (2013).
6. Goodman, A. L. *et al.* Identifying genetic determinants needed to establish a human gut symbiont in its habitat. *Cell Host Microbe* **6,** 279–289 (2009).
7. Nollmann, F. I. *et al.* A *Photorhabdus* Natural Product Inhibits Insect Juvenile Hormone Epoxide Hydrolase. *Chembiochem* **16,** 766–771 (2015).
8. Lorenzen, W., Ahrendt, T., Bozhueyuek, K. A. J. & Bode, H. B. A multifunctional enzyme is involved in bacterial ether lipid biosynthesis. *Nat. Chem. Biol.* **10,** 425–427 (2014).
9. Waters, C. M. & Bassler, B. L. The *Vibrio harveyi* quorum-sensing system uses shared regulatory components to discriminate between multiple autoinducers. *Genes Dev.* **20,** 2754–2767 (2006).
10. Thoma, S. & Schobert, M. An improved *Escherichia coli* donor strain for diparental mating. *FEMS Microbiol. Lett.* **294,** 127–132 (2009).
11. Fischer-Le Saux, M., Viallard, V., Brunel, B., Normand, P. & Boemare, N. E. Polyphasic classification of the genus *Photorhabdus* and proposal of new taxa: *P-luminescens* subsp *luminescens* subsp nov., *P-luminescens* subsp *akhurstii* subsp nov., *P-luminescens* subsp *laumondii* subsp nov., *P.temperata* sp nov., *P-temperata* subsp *temperata* subsp nov and *P-asymbiotica* sp nov. *Int. J. Syst. Bacteriol.* **49,** 1645–1656 (1999).
12. Lengyel, K. *et al.* Description of four novel species of *Xenorhabdus*, family Enterobacteriaceae: *Xenorhabdus budapestensis* sp nov., *Xenorhabdus ehlersii* sp nov., *Xenorhabdus innexi* sp nov., and *Xenorhabdus szentirmaii* sp nov. *Syst. Appl. Microbiol.* **28,** 115–122 (2005).
13. Bode, E. *et al.* Promoter Activation in *Δhfq* Mutants as an Efficient Tool for Specialized Metabolite Production Enabling Direct Bioactivity Testing. *Angew. Chem. Int. Ed. Engl.* **58,** 18957–18963 (2019).
14. Joyce, S. A. *et al.* Bacterial biosynthesis of a multipotent stilbene. *Angew. Chem. Int. Ed. Engl.* **47,** 1942–1945 (2008).
15. Brachmann, A. O. *et al.* A type II polyketide synthase is responsible for anthraquinone biosynthesis in *Photorhabdus luminescens*. *Chembiochem* **8,** 1721–1728 (2007).
16. Bode, H. B. *et al.* Determination of the Absolute Configuration of Peptide Natural Products by Using Stable Isotope Labeling and Mass Spectrometry. *Chemistry* **18,** 2342–2348 (2012).
17. Brachmann, A. O. *et al.* Pyrones as bacterial signaling molecules. *Nat. Chem. Biol.* **9,** 573–578 (2013).
18. Brachmann, A. O., Forst, S., Furgani, G. M., Fodor, A. & Bode, H. B. Xenofuranones A and B: Phenylpyruvate dimers from *Xenorhabdus szentirmaii*. *J. Nat. Prod.* **69,** 1830–1832 (2006).
19. Zhou, Q. *et al.* Structure and Biosynthesis of Xenoamicins from Entomopathogenic *Xenorhabdus*. *Chemistry* **19,** 16772–16779 (2013).
20. Cai, X. *et al.* Entomopathogenic bacteria use multiple mechanisms for bioactive peptide library design. *Nat Chem* **9,** 379–386 (2017).
21. Corpet, F. Multiple sequence alignment with hierarchical clustering. *Nucleic Acids Res.* **16,** 10881–10890 (1988).